Stochastic phase resetting of stimulus-locked responses of two coupled oscillators: Transient response clustering, synchronization, and desynchronization

Peter A. Tass

Citation: Chaos **13**, 364 (2003); doi: 10.1063/1.1505813
View online: https://doi.org/10.1063/1.1505813
View Table of Contents: http://aip.scitation.org/toc/cha/13/1
Published by the American Institute of Physics

Stochastic phase resetting of stimulus-locked responses of two coupled oscillators: Transient response clustering, synchronization, and desynchronization

Peter A. Tass[a)]
Institute of Medicine, Research Centre Jülich, D-52425 Jülich, Germany
and Department of Stereotactic and Functional Neurosurgery, University of Cologne, Germany

(Received 17 April 2002; accepted 17 July 2002; published 21 February 2003)

Transient phase dynamics, synchronization, and desynchronization which are stimulus-locked (i.e., tightly time-locked to a repetitively administered stimulus) are studied in two coupled phase oscillators in the presence of noise. The presented method makes it possible to detect such processes in numerical and experimental signals. The time resolution is enormous, since it is only restricted by the sampling rate. Stochastic stimulus locking of the phases or the $n:m$ phase difference at a particular time t relative to stimulus onset is defined by the presence of one or more prominent peaks in the cross-trial distribution of the phases or the $n:m$ phase difference at time t relative to stimulus onset in an ensemble of poststimulus responses. The oscillators' coupling may cause a transient cross-trial response clustering of the poststimulus responses. In particular, the mechanism by which intrinsic noise induces symmetric antiphase cross-trial response clustering in coupled detuned oscillators is a stochastic resonance. Unlike the presented approach, both cross-trial averaging (where an ensemble of poststimulus responses is simply averaged) and cross-trial cross correlation (CTCC) lead to severe misinterpretations: Triggered averaging cannot distinguish a cross-trial response clustering or decorrelation from a mean amplitude decrease of the single responses. CTCC not only depends on the oscillators' phase difference but also on their phases and, thus, inevitably displays ''artificial'' oscillations that are not related to synchronization or desynchronization.
 [DOI: 10.1063/1.1505813]

Transient responses of coupled oscillators to pulsatile stimuli are relevant in several fields of the natural sciences. Such responses are typically studied by experimentalists to obtain information on dynamical systems and to characterize the system's inventory of reactions. For example, in neurology stimulus evoked electroencephalography responses are a standard tool for diagnosis. The data analysis tools typically used to investigate such responses aim at a noise reduction, e.g., by means of particular averaging techniques, in order to reveal what is supposed to be the actual response to the stimulus. Dealing with physiological data, it is indispensable to take into account noise inherent in the dynamics. This type of noise, however, is not just something one should try to get rid of at all costs. For example, if coupled oscillators may react to a stimulus in more than one way due to intrinsic noise, it does not make sense to apply data analysis methods designed to extract only one sterotyped response. This article explains how complex transient responses of two coupled oscillators emerge as a consequence of the oscillators' interactions in the presence of noise. In analogy to multistability in stationary processes, multistability of transient stimulus induced responses may occur. In detuned oscillators intrinsic noise induces a cross-trial response clustering in a stochastic resonance-like manner. The article presents a simple model of two coupled phase oscillators subject to noise. The novel dynamical stimulus induced phenomena demonstrate why the assumptions behind the standard data analysis tools are dangerous and even misleading. Furthermore, a data analysis technique is presented which makes it possible to detect complex responses of two coupled oscillators to stimulation in a reliable way. In particular, this work makes it possible to detect a transient clustering of coordinated short-term responses. Processes of this kind might be particularly important in the context of short-term adaptation during sensory processing.

I. INTRODUCTION

Synchronization is of great importance in physics,[1] chemistry,[2] biology,[3] neuroscience,[4] and medicine.[5,6] A large number of studies addressed stochastic phase synchronization of periodic oscillators[2,1] and chaotic oscillators[7,8] in physics[1,9] and biology.[10,11] The majority of these studies focused on stationary dynamics evolving on a long time scale, i.e., for time $t \to \infty$. Stochastic phase synchronization was defined as appearance of one or more prominent peaks in the distribution of the phase difference during a sufficiently long observation.[1,12]

Numerous physical processes, however, are caused by pulsatile stimuli and are transient. They act on short time scales and fulfill neither a $t \to \infty$ nor a quasistationarity assumption. The analysis of transient bivariate data is a crucial

[a)]Electronic mail: P.Tass@fz-juelich.de

issue in various fields of the natural sciences. For example, transient short-term brain responses evoked by sensory stimuli play a key role in the study of cerebral information processing and diagnosis.[6] Up to now, a stimulus-locked response of a neuronal population is typically analyzed with a cross-trial averaging (CTA), where an ensemble of post-stimulus responses is averaged across trials.[13,14] To study the oscillators' interaction, cross-trial averaged responses of two neuronal oscillators are phenomenologically analyzed, e.g., by comparing changes of peak latencies or amplitudes under varying conditions. In addition to CTA, a cross-trial cross-correlation (CTCC), i.e., a cross-correlation calculated across all trials at each time t relative to stimulus onset, may be used to detect linear correlations in an ensemble of pairs of responses.

Based on a stochastic phase resetting approach,[5] I present a method for the analysis of stimulus-locked transient phase dynamics, synchronization and desynchronization of two oscillators subject to noise. Stochastic stimulus locking of the phase dynamics and stochastic stimulus-locked $n:m$ phase synchronization is characterized by the presence of one or more prominent peaks in the cross-trial distribution of the phases and of the $n:m$ phase difference at each time t relative to stimulus onset in an ensemble of responses. The time resolution of this method is only restricted by the sampling rate. In contrast, both CTA (Refs. 13, 14) and CTCC lead to misinterpretations or even artifacts. A part of the results of this study was already presented in a rapid communication.[15]

II. STOCHASTIC MODEL

We consider two phase oscillators with phases ψ_1, ψ_2 and constant amplitudes, given by

$$\dot{\psi}_j = \omega_j - K \sin(\psi_j - \psi_k) + X(t)\, S_j(\psi_j) + F_j(t), \tag{1}$$

where $j,k=1,2$ and $j \neq k$. The eigenfrequencies read $\omega_{1,2} = \omega \pm \mu/2$ with detuning μ. The stimuli are modelled by 2π-periodic, time independent functions $S_j(\psi_j) = S_j(\psi_j + 2\pi)$, since in biology the effect of a stimulus is typically phase dependent.[3] Both stimuli are delivered simultaneously. Switching on and off the stimuli is modelled by

$$X(t) = \begin{cases} 1: & \text{stimulus is on at time } t \\ 0: & \text{stimulus is off at time } t. \end{cases} \tag{2}$$

The random forces F_1 and F_2 are Gaussian white noise fulfilling $\langle F_j(t) \rangle = 0$ and $\langle F_j(t) F_k(\tilde{t}) \rangle = D\,\delta_{jk}\,\delta(t-\tilde{t})$ with constant noise amplitude D. Equation (1) may serve as a minimal model for two electrically stimulated neurons[5] or as a minimal model for two neuronal populations affected by sensory stimuli (see below). We set the amplitude of both oscillators equal to 1 and define the signal of the jth phase oscillator as

$$x_j(t) = \cos \psi_j(t). \tag{3}$$

III. CROSS-TRIAL ANALYSIS BASED ON STOCHASTIC PHASE RESETTING

Normalized phases,

$$\phi_j(t) = \frac{\psi_j(t)}{2\pi} \bmod 1 \quad (j=1,2) \tag{4}$$

and the *normalized cyclic $n:m$ phase difference,*

$$\varphi_{n,m}(t) = \frac{n\psi_1(t) - m\psi_2(t)}{2\pi} \bmod 1 \tag{5}$$

are introduced. We want to detect whether in an ensemble of responses to the stimulus there are epochs during which the phases ϕ_1, ϕ_2 and/or the phase difference $\varphi_{n,m}$ display a stereotyped, tightly stimulus-locked time course. For this, we deliver a series of l identical stimuli at random times τ_1, $\tau_2, \ldots, \tau_l$. The length of the interstimulus intervals is randomized according to

$$\tau_{k+1} - \tau_k = w + \zeta_k, \tag{6}$$

where w is constant and large compared to the time scale of the transient dynamics, and ζ_k is uniformly distributed in $[0, 2\pi/\Omega]$. To each stimulus we attach an identical time window $[t_a, t_b]$ ($t_a<0$, $t_b>0$, Fig. 1). Each window has a time axis t', so that $t' \in [t_a, t_b]$, where the onset of the stimulus in each window lies in $t'=0$. The window length $t_b - t_a$ is smaller than the length of the interstimulus intervals: $t_b - t_a < w$.

For the sake of simplicity we drop the prime in t', keeping in mind that from now on t denotes the window's time axis. To study the dynamics of the ensemble of stimulus-locked responses for each time $t \in [t_a, t_b]$ we introduce the time-dependent *cross-trial (CT) distributions* of the normalized phases from Eq. (4) and the cyclic $n:m$ phase difference from Eq. (5) by

$$\{\phi_j(t+\tau_k)\}_{k=1,\ldots,l}, \quad \{\varphi_{n,m}(t+\tau_k)\}_{k=1,\ldots,l}. \tag{7}$$

The time course of ϕ_j and $\varphi_{n,m}$ is perfectly stimulus-locked at time t if the corresponding CT distributions from Eq. (7) are Dirac-type distributions, i.e., $\phi_j(t+\tau_i) = \phi_j(t+\tau_k)$ and $\varphi_{n,m}(t+\tau_i) = \varphi_{n,m}(t+\tau_k)$ for all $i,k=1,\ldots,l$. On the other hand, if ϕ_j and $\varphi_{n,m}$ are not at all stimulus-locked at time t, these distributions are uniform. To quantify the extent of stimulus locking of ϕ_j and $\varphi_{n,m}$ for each time t, we introduce the time-dependent *stimulus locking indices* $\lambda_j^{(\nu)}(t)$ of ϕ_j with

$$\lambda_j^{(\nu)}(t) = \left| \frac{1}{l} \sum_{k=1}^{l} \exp[i\nu 2\pi \phi_j(\tau_k + t)] \right|, \tag{8}$$

and the *$n:m$ stimulus locking indices* $\sigma_{n,m}^{(\nu)}(t)$ of $\varphi_{n,m}$ by

$$\sigma_{n,m}^{(\nu)}(t) = \left| \frac{1}{l} \sum_{k=1}^{l} \exp[i\nu 2\pi \varphi_{n,m}(\tau_k + t)] \right|, \tag{9}$$

where $|y|$ denotes the modulus of y, and ν is an integer. $\lambda_j^{(\nu)}(t)$ and $\sigma_{n,m}^{(\nu)}(t)$ detect whether ϕ_j's or $\varphi_{n,m}$'s CT distribution from Eq. (7) at time t has ν peaks that are equally spaced in $[0,1]$ (modulo 1) and fulfill $0 \leqslant \lambda_j^{(\nu)}(t) \leqslant 1$, $0 \leqslant \sigma_{n,m}^{(\nu)}(t) \leqslant 1$ for $t \in [t_a, t_b]$ and for all integers ν.

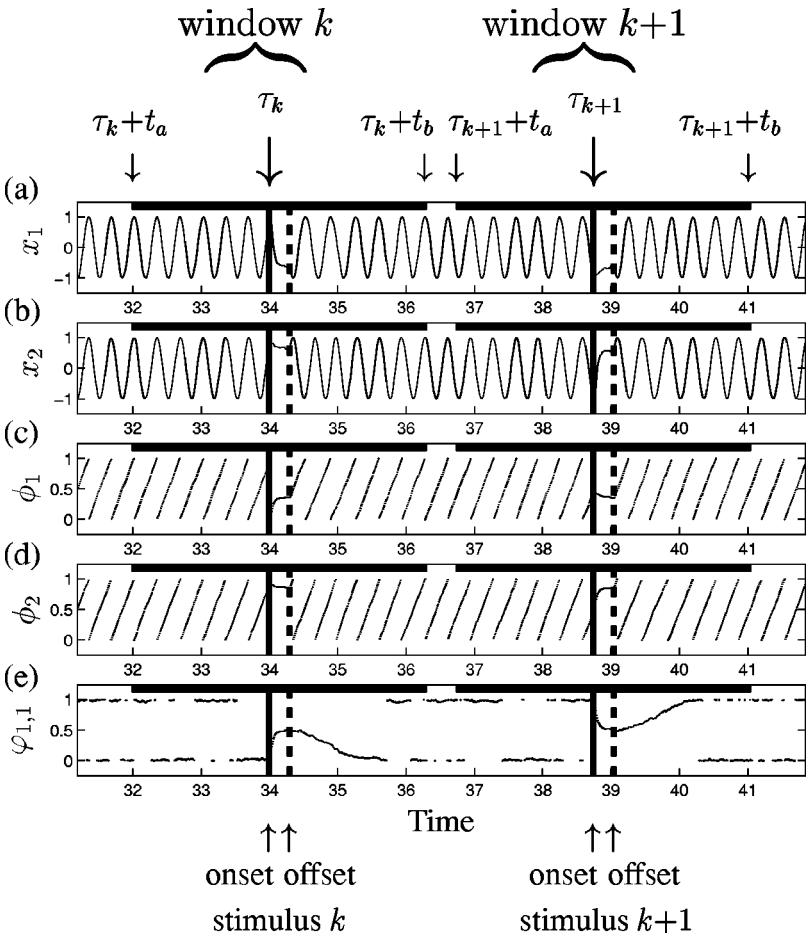

FIG. 1. Scheme illustrating the cross-trial analysis: A series of l identical stimuli is administered at random times $\tau_1, \tau_2, \ldots, \tau_l$. Begin and end of the stimuli are denoted by bold solid and dashed vertical lines, respectively. An identical time window $[t_a, t_b]$ (with $t_a<0$, $t_b>0$) is attached to each stimulus and indicated by a shaded region at the top of each panel. The signals $x_1(t)=\cos[2\pi\phi_1(t)]$ and $x_2(t)=\cos[2\pi\phi_2(t)]$ from (3) are shown in (a) and (b). The corrsponding phases ϕ_1 and ϕ_2 from (4) are displayed in (c) and (d). The normalized cyclic 1:1 phase difference $\varphi_{1,1}$ from (5) is shown in (e). Note that $\varphi_{1,1}=0$ and $\varphi_{1,1}=1$ are identical, which is why continuous variations around $\varphi_{1,1}=0$ appear as abrupt jumps between 0 and 1. The traces shown stem from a numerical integration of the model Eq. (1), which is described in Fig. 2.

(i) One, (ii) two or (iii) three equally spaced peaks in the distribution $\{\phi_j(t+\tau_k)\}_{k=1,\ldots,l}$ at time t correspond to (i) large $\lambda_j^{(\nu)}(t)$ for $\nu=1,2,3$, (ii) large $\lambda_j^{(2)}(t)$ and small $\lambda_j^{(\nu)}(t)$ for $\nu=1,3$, (iii) large $\lambda_j^{(3)}(t)$ and small $\lambda_j^{(\nu)}(t)$ for $\nu=1,2$. $\lambda_j^{(\nu)}$ and $\sigma_{n,m}^{(\nu)}$ are the modulus of the νth Fourier mode of the CT distributions from Eq. (7) (cf. Ref. 5). Similar to Eq. (8), $Z_\nu(t)=l^{-1}\Sigma_{k=1}^{l}\exp[i\nu\xi_k(t)]$ detects ν phase-locked clusters in a population of l oscillators with phases $\xi_1,\ldots,\xi_l$.[5,16]

We use the first and the 99th percentile of the prestimulus distributions $\{\lambda_j^{(\nu)}(t)\}_{t\in[t_a,0[}$ and $\{\sigma_{n,m}^{(\nu)}(t)\}_{t\in[t_a,0[}$ as confidence levels in order to determine whether a stimulus causes a significant increase or decrease of $\lambda_j^{(\nu)}$ or $\sigma_{n,m}^{(\nu)}$. An increase or a decrease of the stimulus locking of ϕ_j at time t is considered significant provided $\lambda_j^{(1)}(t)$ is larger than the 99th or smaller than the first percentile of $\{\lambda_j^{(1)}(t)\}_{t\in[t_a,0[}$, respectively. Significant stimulus-locked in-phase synchronization or desynchronization at time t occurs provided $\sigma_{n,m}^{(1)}(t)$ exceeds the 99th or falls below the first percentile of $\{\sigma_{n,m}^{(1)}(t)\}_{t\in[t_a,0[}$.

IV. TRANSIENT RESPONSE CLUSTERING, SYNCHRONIZATION, AND DESYNCHRONIZATION

We here focus on the simplest case with $n=m=1$. Let us consider the effect of stimuli of first order with equal intensity defined by

$$S_1(\psi_1)=I\cos\psi_1, \quad S_2(\psi_2)=I\cos(\psi_2+\pi) \tag{10}$$

(Figs. 2 and 3). We assume that the coupling is strong enough compared to the noise amplitude D, so that without stimulation the two oscillators spontaneously synchronize in-phase [Figs. 2(f), 2(g)]. The stimulation intensity I is large compared to the coupling strength K and to the noise amplitude D ($K\ll I$, $D\ll I$). The two strong stimuli quickly reset the oscillators: ϕ_1 is shifted close to $\phi_1^{\text{stat}}\approx 0.36$ [Fig. 2(a)], whereas ϕ_2 is forced close to $\phi_2^{\text{stat}}=\phi_1^{\text{stat}}+0.5\approx 0.86$ because of the phase shift of π in the argument of S_2 [Fig. 2(d)].

The reset of the oscillators' phases is reflected by an increase of the locking index $\lambda_j^{(1)}$ [Fig. 2(b)]. Due to this reset the oscillators undergo a transition from an in-phase synchronization to a particularly strong antiphase synchronization via a transient desynchronization in between [Figs. 2(f), 2(g)]. After the stimulation both oscillators relax back to the same in-phase synchronization as before stimulation. During this relaxation they pass through a desynchronization which lasts longer than the desynchronization during stimulation since $K\ll I$. In the course of the desynchronization during and after stimulation the trajectories of $\varphi_{1,1}$ form two "branches" that converge to and diverge from $\varphi_{1,1}=0.5$ [Fig. 2(f)]. The antiphase position of the two branches coincides with a local maximum of $\sigma_{1,1}^{(2)}$ [Fig. 2(h)] and a local minimum of $\sigma_{1,1}^{(1)}$ [Fig. 2(g)].

After the stimulation the trajectories of both ϕ_1 and ϕ_2 form two clusters, respectively: While $\lambda_j^{(1)}$ relaxes to zero, $\lambda_j^{(2)}$ reincreases [Figs. 2(c), 2(e)], which indicates that the

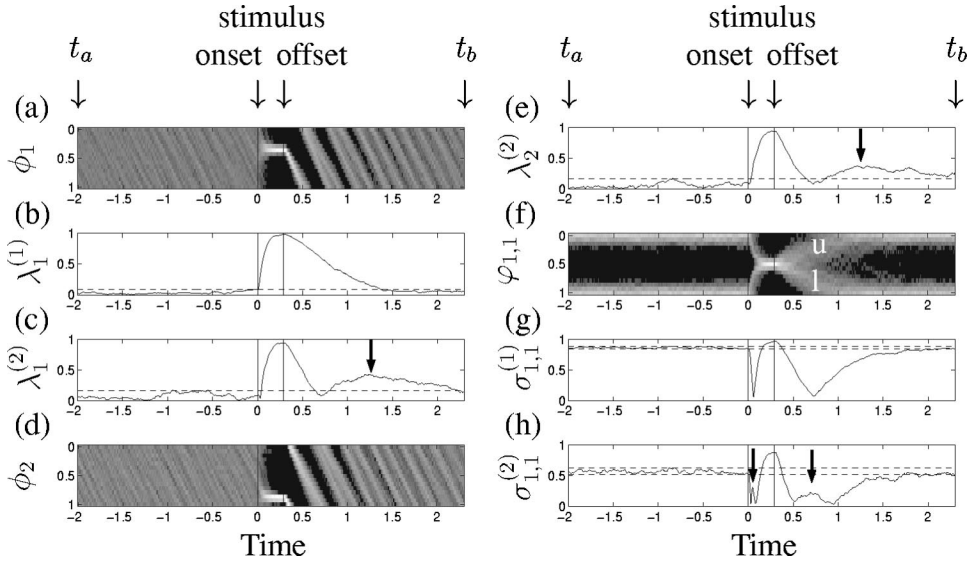

FIG. 2. Strong stimuli $S_1(\psi_1)=I\cos\psi_1$ and $S_2(\psi_2)=I\cos(\psi_2+\pi)$ from Eq. (1) cause an antiphase reset. CT distributions from (7) are shown as time-dependent histograms of ϕ_j and $\varphi_{1,1}$ calculated across trials for each time point relative to stimulus onset within the time window $[t_a,t_b]$: $\{\phi_1(t+\tau_k)\}_{k=1,\ldots,l}$ in (a), $\{\phi_2(t+\tau_k)\}_{k=1,\ldots,l}$ in (d), $\{\varphi_{1,1}(t+\tau_k)\}_{k=1,\ldots,l}$ in (f). (0 is black and maximal values are white.) "u" and "l" indicate upper and lower branch of trajectories in (f). Locking indices from Eqs. (8) and (9): $\lambda_1^{(1)}$ in (b), $\lambda_1^{(2)}$ in (c), and $\lambda_2^{(2)}$ in (e). $\lambda_2^{(1)}$ nearly coincides with $\lambda_1^{(1)}$. $\sigma_{1,1}^{(1)}$ in (g) and $\sigma_{1,1}^{(2)}$ in (h). Local maxima ("↓") of $\lambda_1^{(2)}$, $\lambda_2^{(2)}$, and $\sigma_{1,1}^{(2)}$ indicate antiphase clustering of the corresponding distributions [cf. Figs. 3(a), 3(d)]. Begin (at $t=0$) and end of the stimulation are indicated by vertical lines. Prestimulus interval: $t<0$; poststimulus interval: $t>0$. Significance levels: Dashed lines in (b), (c), and (e) denote the 99th percentile of the prestimulus distributions $\{\lambda_1^{(\nu)}(t)\}_{t\in[-2,0[}$. In (g) and (h) the upper and lower dashed line indicate the 99th and the first percentile of $\{\sigma_{1,1}^{(\nu)}(t)\}_{t\in[-2,0[}$. Parameters of Eq. (1): $K=2$, $\omega=6\pi$, $\mu=0.04$, $D=1$, $I=30$, $w=4$ [cf. Eq. (6)], stimulus duration $=0.3$, number of stimuli $l=200$. In this article the model given by Eq. (1) is numerically solved with a fourth-order Runge–Kutta method. Results are stable with respect to variations of l between 50 and 2000 and more.

distribution $\{\phi_j(t_1+\tau_k)\}_{k=1,\ldots,l}$ has two separate peaks [Figs. 3(a), 3(d)]. With further increasing time the clustering of ϕ_j's trajectories vanishes due to the noise. The intimate relationship between resynchronization and clustering of the trajectories of ϕ_j is reflected by the strongly correlated reincrease of $\lambda_j^{(2)}$ and $\sigma_{1,1}^{(1)}$ (starting at $t\approx 0.75$) [Figs. 2(c), 2(e), 2(g)].

To clarify the relationship between the branching of $\varphi_{1,1}$ and the clustering of ϕ_1 and ϕ_2, we split the ensemble of l trajectories of $\varphi_{1,1}$ into the two subsets U and L belonging to the upper and lower branch of $\varphi_{1,1}$ during strongest antiphase branching [at time $t_0\approx 0.75$, Figs. 2(f), 2(g)]: $\varphi_{1,1}(t_0+\tau_k)\leqslant 0.5$ for $k\in U$ and $\varphi_{1,1}(t_0+\tau_k)>0.5$ for $k\in L$. [Note, due to the graphics program used, in Fig. 2(f) the y-axis runs downwards, so that values of $\varphi_{1,1}$ in the upper branch are smaller than those in the lower branch.] If in a single response $\varphi_{1,1}$ runs through the upper branch at time $t_0\approx 0.75$ both ϕ_1 and ϕ_2 preferably end up in the right peak of their distributions at time $t_1\approx 1.25$ [Figs. 3(b), 3(e)]. In contrast, if $\varphi_{1,1}$ runs through the lower branch ϕ_1 as well as ϕ_2 are mainly found in the left peak of their distributions at time $t_1\approx 1.25$ [Figs. 3(c), 3(f)]. The peaks in the distributions of ϕ_1 and ϕ_2 which belong to the upper branch [Figs. 3(b), 3(e)] or the lower branch [Figs. 3(c), 3(f)] are approximately in-phase, respectively.

V. COMPARISON WITH CROSS-TRIAL AVERAGING

To perform a cross-trial average of the signal x_j from Eq. (3) of the jth phase oscillator, we use the stimulus onset τ_k as trigger. The *cross-trial averaged signal* reads

$$\overline{x_j}(t)=\frac{1}{l}\sum_{k=1}^{l} x_j(\tau_k+t). \tag{11}$$

The assumption behind the triggered averaging is that a response x_j can be decomposed into a stereotyped evoked response e_j occurring with a constant delay after the stimulus, and additive Gaussian noise ξ_j, so that

$$x_j(\tau_k+t)=e_j(t)+\xi_j(\tau_k+t) \tag{12}$$

holds.[13,14] Averaging then improves the signal-to-noise ratio by $\sqrt{l}$, where the number of responses l typically equals 20–300, and $\overline{x_j}(t)\to e_j(t)$ for $l\to\infty$.[13,14]

The assumption from Eq. (12) is, of course, not justified for the stochastic model given by Eq. (1), because the oscillators perform an ongoing oscillation, the stimulation effect depends on the phase of the oscillator, and the model's noise is not simply added to the signal x_j, but inherent in the dynamics. Anyhow, the model given by Eq. (1) has basic features in common with stimulated brain activity: (i) Ongoing oscillations abound in the brain.[17] (ii) Evoked responses result from reorganizing part of these ongoing oscillations, in particular, by resetting their phase dynamics.[18,19] For example, auditory stimuli cause an evoked EEG response mainly by changing the phases (but not the amplitudes) of the Fourier spectrum of the existing, spontaneous neuronal oscillatory activity.[18] (iii) Noise is inevitably inherent in neuronal action.[20] Hence, also in neuroscience the averaging assumption is highly questionable. Nevertheless, averaging is

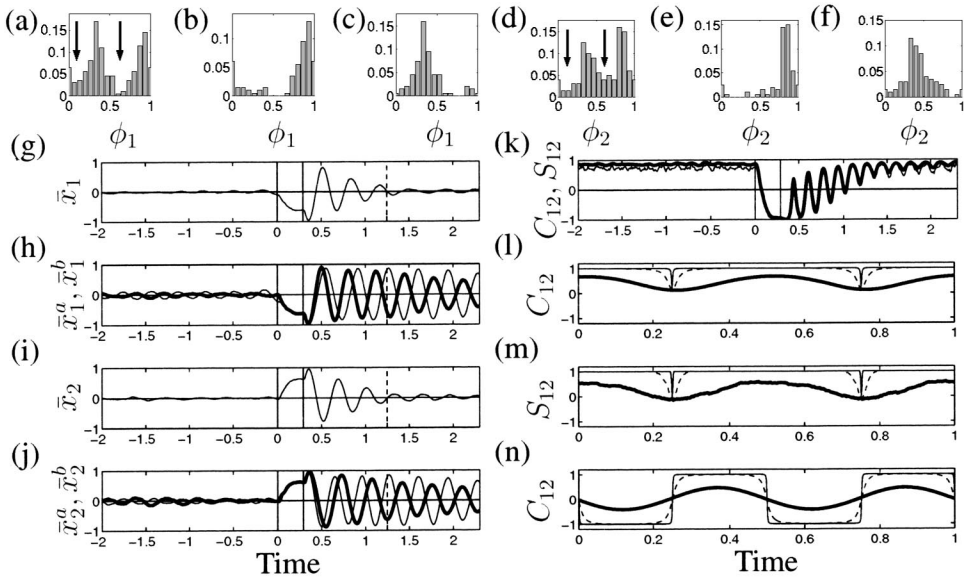

FIG. 3. Clustering of the responses, averaged signals, and CTCC for the simulation of Fig. 2. Antiphase clustering of the distributions $\{\phi_1(t_1+\tau_k)\}_{k=1,\ldots,l}$ in (a) and $\{\phi_2(t_1+\tau_k)\}_{k=1,\ldots,l}$ in (d) (peaks separated by "↓") at time $t_1 \approx 1.25$, when period 2 measures $\lambda_1^{(2)}$ and $\lambda_2^{(2)}$ are locally maximal [Figs. 2(c), 2(e)]. At time $t_0 \approx 0.75$ the "branches" of $\varphi_{1,1}$ in Fig. 2(f) are in antiphase position [$\sigma_{1,1}^{(2)}$ is locally maximal]. U and L denote the subsets of trials for that $\varphi_{1,1}(t_0+\tau_k)$ is in the upper and lower branch ["u" and "l" in Fig. 2(f)]: $\varphi_{1,1}(t_0+\tau_k) \leqslant 0.5$ for $k \in U$ and $\varphi_{1,1}(t_0+\tau_k) > 0.5$ for $k \in L$. Distributions of ϕ_1 and ϕ_2 belonging to the two branches of $\varphi_{1,1}$: $\{\phi_1(t_1+\tau_k)\}_{k\in U}$ in (b), $\{\phi_2(t_1+\tau_k)\}_{k\in U}$ in (e), $\{\phi_1(t_1+\tau_k)\}_{k\in L}$ in (c), and $\{\phi_2(t_1+\tau_k)\}_{k\in L}$ in (f). Cross-trial averaged signals $\overline{x_1}$ in (g) and $\overline{x_2}$ in (i) according to Eq. (11). (h) Averaging those $x_1(\tau_k+t)$ that belong to the left and right peak of the distribution in (a) separately, yields the averaged signals $\overline{x_1^a}$ (thick line) and $\overline{x_1^b}$ (thin line), respectively. (j) Analogously, $\overline{x_2^a}$ (thick line) and $\overline{x_2^b}$ (thin line) belong to the left and right peak of the distribution in (d). Note that after the stimulation the phase relationship of $\overline{x_j^a}$ and $\overline{x_j^b}$ changes from in-phase to antiphase, so that $\overline{x_j} = (\overline{x_j^a} + \overline{x_j^b})/2$ vanishes rapidly, whereas both $\overline{x_j^a}$ and $\overline{x_j^b}$ relax slowly. Dashed line in (g)–(j) at time $t_1 \approx 1.25$. (k) C_{12} (thick line) and S_{12} (thin line) display "artificial" oscillations with twice the oscillators' frequency [cf. (h), (j)]. Format in (g)–(k) as in Fig. 2. CTCC and CTSCC, i.e., C_{12} from Eq. (13) and S_{12} from Eq. (14) produce severe artifacts. To demonstrate the origin of CTCC's and CTSCC's "artificial" oscillations we study noise-free, idealized responses which are defined by Eqs. (15) and (16) [but not generated by the model from Eq. (1)]: (l), (m): An ensemble of responses with in-phase synchronized phases, where $\phi_1(t+\tau_k) = [t+\varepsilon\xi_{1,k}] \bmod 1$ and $\phi_2(t+\tau_k) = [t+\Delta\phi+\varepsilon\xi_{2,k}] \bmod 1$ with $\Delta\phi = 0$ for $k = 1,\ldots,l$, where $\{\xi_{j,k}\}_{k=1}^{l}$ is constant and normally distributed with variance 1, and $\varepsilon = 0.01$ (thin line), 0.1 (dashed line), 1 (bold line). Note, ϕ_1 and ϕ_2 have period 1. For $\varepsilon = 0$, C_{12} and S_{12} are always = 1, except for the times when the signals $x_j = \cos(2\pi\phi_j)$ vanish. A constant gitter of the phases ($\varepsilon > 0$) smoothens the nearly coinciding C_{12} and S_{12}, so that oscillations with twice the oscillators' frequency occur—although the phase difference $\varphi_{n,m}$ of all pairs of responses is constant. (n) C_{12} of an ensemble of responses as in (l) but with $\Delta\phi = 0.25$, where $\varepsilon = 0.01$ (thin line), 0.1 (dashed line), 1 (bold line).

widely used for noise-reduction of electroencephalography (EEG) (Refs. 6, 13) and magnetoencephalography (MEG) signals[14,17] and local field potentials (LFP).[4]

The clustering of ϕ_1 and ϕ_2 has an important effect on the cross-trial averaged responses $\overline{x_1}$ and $\overline{x_2}$. Before the stimulation $\overline{x_1}$ and $\overline{x_2}$ vanish due to the randomized stimulus administration [Figs. 3(g), 3(i)]. The stimuli reset ϕ_1 and ϕ_2, and hence $\overline{x_1}$ and $\overline{x_2}$ approach a constant value. After the stimulation $\overline{x_1}$ and $\overline{x_2}$ display strongly damped oscillations. This strong damping is due to the clustering in the ensemble of responses of ϕ_1 and ϕ_2. Averaging the signals belonging to the right and to the left peak of the distribution of ϕ_j [Figs. 3(a), 3(d)] separately, yields the slowly relaxing averaged signals $\overline{x_j^a}$ and $\overline{x_j^b}$ [Figs. 3(h), 3(j)]. $\overline{x_j} = (\overline{x_j^a} + \overline{x_j^b})/2$ vanishes rapidly since within only two cycles after the stimulation the phase relationship between $\overline{x_j^a}$ and $\overline{x_j^b}$ turns from in-phase into antiphase. From Figs. 3(a)–3(f) we read off that $\overline{x_j^a}$ mainly belongs to $\varphi_{1,1}$'s upper branch, whereas $\overline{x_j^b}$ mainly belongs to $\varphi_{1,1}$'s lower branch. While $\overline{x_j^a}$ and $\overline{x_j^b}$ establish an antiphase relation, both pairs $\overline{x_1^a}$ and $\overline{x_2^a}$ as well as $\overline{x_1^b}$ and $\overline{x_2^b}$ get in-phase [Figs. 3(h), 3(j)].

To illustrate the impact of the type of reset on $\overline{x_j}$, we replace the second stimulus by $S_2(\psi_2) = I\cos(\psi_2+\gamma)$ with constant γ, while all other parameters are as in Fig. 2. In a series of simulations we vary γ within $[0,2\pi]$, to cover the whole spectrum between in-phase resetting ($\gamma = 0$ or 2π) and antiphase resetting ($\gamma = \pi$). Only in a narrow phase range around $\gamma = \pi$ the averaged responses $\overline{x_j}$ vanish rapidly [Figs. 4(a), 4(d)] due to the transient desynchronization [Fig. 4(e)] and the following clustering of ϕ_j's responses [Figs. 4(b), 4(c)]. In contrast, if no antiphase reset is achieved, i.e., if γ is not close to π, the stimuli mainly strengthen the in-phase synchronization temporarily [Fig. 4(e)]. In this case no desynchronization [Fig. 4(e)] and no clustering [Figs. 4(b), 4(c)] occur, so that $\overline{x_j}$ vanishes slowly [Figs. 4(a), 4(d)].

Let us interpret the dynamics of $\overline{x_j}$ in the spirit of the evoked response literature.[6,13,14] Before stimulation the oscillators are not active, the stimulus activates them, and their activity (i.e., amplitude of $\overline{x_j}$) fades away quickly (for γ close to π) or slowly (else) [Figs. 4(a), 4(d)]. However, according to Eq. (1) the oscillators are permanently active with constant amplitude, irrespective of γ. For γ close to π the averaged responses $\overline{x_j}$ rapidly relax to zero due to the poststimulus response decorrelation [Figs. 3(h), 3(j)]. Cross-trial averaging[13,14] cannot distinguish between a mean amplitude decrease of the single responses and a response decorrelation. In contrast, this is possible with the stochastic phase resetting analysis presented here.

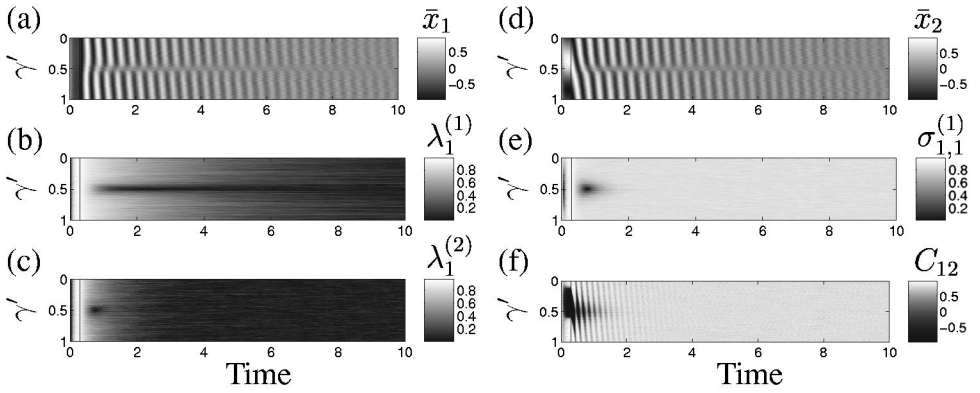

FIG. 4. In a series of simulations $\gamma' = \gamma/(2\pi)$ is varied within [0,1], where $S_2(\psi_2) = I\cos(\psi_2 + \gamma)$, and all other parameters as in Fig. 2. Time course of $\overline{x_1}$ from Eq. (11) in (a), $\lambda_1^{(1)}$ from Eq. (8) in (b), $\lambda_1^{(2)}$ in (c), $\overline{x_2}$ in (d), $\sigma_{1,1}^{(1)}$ from Eq. (9) in (e), and C_{12} from Eq. (13) in (f) (0 is black and maximal values are white). $\lambda_2^{(j)}$ nearly coincide with $\lambda_1^{(j)}$. The transient antiphase response clustering, characterized by a reincreasing $\lambda_j^{(2)}$ and vanishing $\lambda_j^{(1)}$ [Figs. 2(b), 2(c), 2(e)], only occurs for γ close to π. Stimulation starts at $t=0$; the end of the stimulation is indicated by the vertical line.

VI. COMPARISON WITH CROSS-TRIAL CROSS-CORRELATION

To detect linear correlations between the two oscillators across trials we apply the cross-correlation[21] across trials to either the signals or the signals' signs.

$$C_{12}(t) = \frac{\Sigma_{k=1}^{l} x_1(t+\tau_k)x_2(t+\tau_k)}{\sqrt{[\Sigma_{k=1}^{l} x_1^2(t+\tau_k)][\Sigma_{k=1}^{l} x_2^2(t+\tau_k)]}} \tag{13}$$

is the *cross-trial cross-correlation (CTCC)* between x_1 and x_2 at time t, which (to avoid a singularity) by definition is set$=0$ if all responses of x_1 or x_2 vanish at time t. To avoid singular behavior, alternatively, we may also use the *cross-trial sign cross-correlation (CTSCC)*,

$$S_{12}(t) = \frac{1}{l}\sum_{k=1}^{l} \mathrm{sign}[x_1(t+\tau_k)x_2(t+\tau_k)] \tag{14}$$

which corresponds to the CTCC of the signals' signs, where $\mathrm{sign}(a) = -1$, 0 or 1 if $a<0, =0$ or >0.

Both C_{12} and S_{12} are normalized: $-1 \leqslant C_{12}(t) \leqslant 1$ and $-1 \leqslant S_{12}(t) \leqslant 1$ hold for all t. $C_{12}(t)=1$ or -1 if $x_1(t+\tau_k) = cx_2(t+\tau_k)$ with constant $c>0$ or <0 for all $k=1,\ldots,l$. Analogously, $S_{12}(t)=1$ or -1 if $x_1(t+\tau_k)$ and $x_2(t+\tau_k)$ have either the same sign for all $k=1,\ldots,l$ or different sign for all $k=1,\ldots,l$. $S_{12}(t)=0$ if at least one of the responses vanishes at time t for all $k=1,\ldots,l$ [Figs. 3(l)–3(n)].

Although different by definition, CTCC and CTSCC are very similar and do not only depend on the phase difference $\varphi_{n,m}$, but inevitably also on the oscillators' absolute phases ϕ_j. This is illustrated in Figs. 3(l)–3(n) by means of noise-free, idealized responses. The latter are not generated by the model given by Eq. (1), but simply defined in order to reveal crucial features of CTCC and CTSCC. Imagine an ensemble of responses of both oscillators defined by

$$\phi_1(t+\tau_k) = [t + \varepsilon\xi_{1,k}] \mod 1, \tag{15}$$

$$\phi_2(t+\tau_k) = [t + \Delta\phi + \varepsilon\xi_{2,k}] \mod 1, \tag{16}$$

for $k=1,\ldots,l$, where $\Delta\phi$ is the mean phase difference between the responses of the two oscillators, and $\{\xi_{j,k}\}_{k=1}^{l}$ is constant and normally distributed with variance 1 for $j=1,2$. By varying ε we modify the variance of the normal distributions of the responses. Note, the phase difference $\varphi_{1,1}(t+\tau_k)$ of all responses $k=1,\ldots,l$ is invariant with respect to variations of time t. This is the very feature motivating the definition of the synthetic responses from Eqs. (15) and (16). CTCC and CTSCC of these synthetic stimulus-locked responses "artificially" oscillate with increasing time t, i.e., with increasing phases ϕ_j although the phase difference $\varphi_{n,m}$ remains constant. These oscillations occur for all values of the phase difference $\Delta\phi$ [Fig. 3(l)–3(n)].

Correspondingly, CTCC's and CTSCC's "artificial" oscillations are also observed when CTCC and CTSCC are applied to the simulated data belonging to the model from Eq. (1). In the simulation of Fig. 2, prior to stimulation the oscillators are synchronized with phases that are not stimulus-locked due to the randomized stimulation according to Eq. (6). The values of C_{12} and S_{12} are nearly constantly close to 1 [Fig. 3(k)], and correspond to those from Figs. 3(l), 3(m) averaged over one period. The stimulus causes an antiphase reset, so that C_{12} and S_{12} come close to -1. While the stimulus-locked poststimulus responses resynchronize, C_{12} and S_{12} oscillate with twice the oscillators' eigenfrequency [as in Fig. 3(l)–3(n)]. The CTCC is set close to -1 only by an antiphase reset (i.e., for γ close to π), whereas it remains close to 1 else [Fig. 4(f)]. However, independently of the type of reset (i.e., for all γ) the stimulus-locked responses are connected with oscillations of the CTCC that do not reflect synchronization/desynchronization processes. CTSCC displays "artifical" oscillations that are very similar to those of CTCC shown in Fig. 4(f). Hence, CTCC as well as CTSCC are no appropriate measures for stimulus-locked synchronization and desynchronization.

VII. SHAPING STIMULUS-LOCKED RESPONSES

To further demonstrate the important effect of the oscillators' coupling on their cross-trial averaged responses $\overline{x_j}$ we again turn to an antiphase reset of both oscillators, with stimuli as defined by Eq. (10): $S_1(\psi_1) = I\cos(\psi_1)$ and

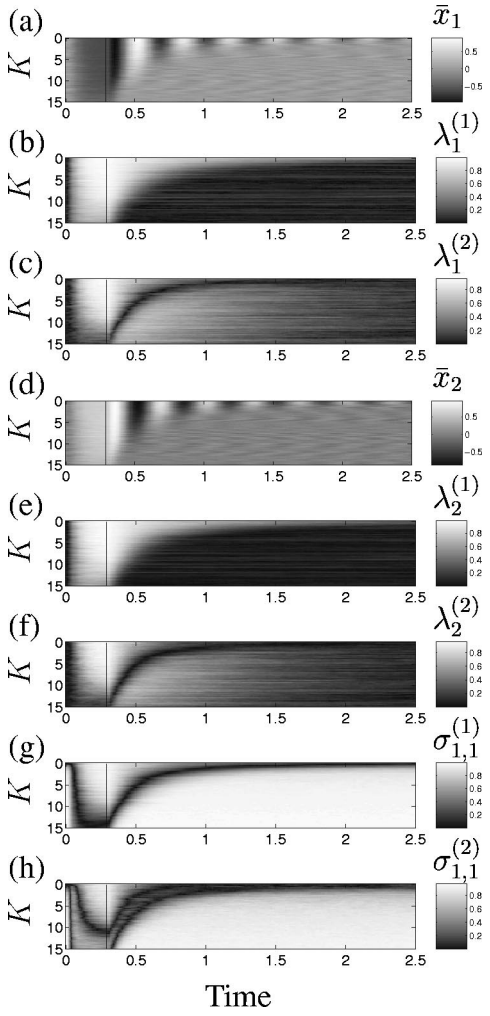

FIG. 5. In a series of simulations the coupling strength K is varied within [0,15], where the antiphase resetting stimuli are given by $S_1(\psi_1)=I\cos(\psi_1)$ and $S_2(\psi_2)=I\cos(\psi_2+\pi)$. All other parameters are as in Fig. 2. Time course of $\overline{x_1}$ from Eq. (11) in (a), $\lambda_1^{(1)}$ from Eq. (8) in (b), $\lambda_1^{(2)}$ in (c), $\overline{x_2}$ in (d), $\lambda_2^{(1)}$ in (e), $\lambda_2^{(2)}$ in (f), $\sigma_{1,1}^{(1)}$ from Eq. (9) in (g), and $\sigma_{1,1}^{(2)}$ in (h) (0 is black and maximal values are white). A pronounced transient antiphase response clustering, with reincreasing $\lambda_j^{(2)}$ and vanishing $\lambda_j^{(1)}$, occurs for sufficiently strong coupling $K>0$ and is connected with strongly damped oscillatory cross-trial averaged responses $\overline{x_j}$, which even vanish for large K. Stimulation starts at $t=0$; the end of the stimulation is indicated by the vertical line.

$S_2(\psi_2)=I\cos(\psi_2+\pi)$. We now vary the coupling strength K from Eq. (1) (Fig. 5). For vanishing coupling the amplitude of $\overline{x_j}$ slowly relaxes, and $\overline{x_j}$ runs through several cycles. Put otherwise, for $K=0$ both oscillators exhibit a pronounced oscillatory cross-trial averaged response. Sufficiently strong coupling $K>0$, however, causes a strong transient antiphase response clustering with reincreasing $\lambda_j^{(2)}$ and vanishing $\lambda_j^{(1)}$. This is related to strongly damped oscillatory cross-trial averaged responses $\overline{x_j}$. For strong enough coupling K the antiphase response clustering occurs so rapidly, that the cross-trial averaged response x_j from Eq. (11) even vanishes.

With increasing coupling strength the transient poststimulus sequence, i.e., desynchronization after stimulation with following resynchronization, combined with the characteristic changes of the indices $\lambda_j^{(k)}$ and $\sigma_{n,m}^{(k)}$ (cf. Fig. 2) occurs on a shorter time scale. The time the oscillators need to undergo this sequence decreases with increasing coupling strength K.

Once more we interpret the dynamics of $\overline{x_j}$ in a way that is typical for evoked response studies.[6,13,14] With increasing coupling strength K duration and amplitude of the response $\overline{x_j}$ decrease and finally vanish. Equating the amplitude of the response $\overline{x_j}$ with the stimulus-locked "activity" of the jth oscillator, we end up with the following interpretation: For sufficiently strong coupling strength K the oscillators no longer become active after having been stimulated. We know, however, that both oscillators are permanently active with constant amplitude 1 (cf. 3). It is the transient antiphase clustering which mimics a weak or even vanishing amplitude of the cross-trial averaged response. Obvioulsy, treating the amplitude of the response $\overline{x_j}$ as equivalent to a stimulus-locked "activity" of the jth oscillator leads to severe misinterpretations. Nevertheless, this way of interpretation is still standard.[6,13,14]

VIII. THE ROLE OF NOISE

A. Motion in a double-well potential

To study the impact of noise on the poststimulus transients we consider the dynamics of the phase difference $\varphi_{1,1}$ that emerges after stimulus administration. According to Eq. (2) we set $X=0$. With $\varphi_{1,1}$ from Eq. (5) and model equation (1) we immediately obtain

$$\dot{\varphi}_{1,1}=\frac{\mu}{2\pi}-\frac{K}{\pi}\sin(2\pi\varphi_{1,1})+F(t)=G(\varphi_{1,1})+F(t). \tag{17}$$

The random forces are given by $F(t)=F_1(t)-F_2(t)$, which is Gaussian white noise obeying $\langle F(t)\rangle=0$ and $\langle F(t)F(\tilde{t})\rangle=2D\delta(t-\tilde{t})$ with constant noise amplitude $2D$. $G(\varphi_{1,1})$ is a shortform for the deterministic terms of the right-hand side of Eq. (17). Studying the poststimulus dynamics of $\varphi_{1,1}$ means considering an initial condition problem of Eq. (17): The stimulus puts $\varphi_{1,1}$ on a particular value, which is $\varphi_{1,1}$'s initial value of the poststimulus period. Starting at that initial value, $\varphi_{1,1}$ relaxes towards a stable state.

First, we consider the behavior occuring without noise, i.e., for $D=0$. In this case the dynamics is governed by a potential

$$V(\varphi_{1,1})=-\int_0^{\varphi_{1,1}}G(\xi)\,\mathrm{d}\xi, \tag{18}$$

which fulfills

$$\dot{\varphi}_{1,1}=-\frac{\mathrm{d}V(\varphi_{1,1})}{\mathrm{d}\varphi_{1,1}} \tag{19}$$

(see Ref. 1 and Chap. 9 in Ref. 22). The dynamics of Eq. (17) corresponds to an overdamped motion of a particle in the potential $V(\varphi_{1,1})$ (Fig. 6). $\varphi_{1,1}$ moves in such a way that it minimizes $V(\varphi_{1,1})$, and $\varphi_{1,1}$ stops only when $\mathrm{d}V/\mathrm{d}\varphi_{1,1}$ vanishes. The maximum of the potential is an unstable fixed point. Let us denote the value of $\varphi_{1,1}$ at which V is maximal by $\varphi_{1,1}^{\max}$. For $\varphi_{1,1}=\varphi_{1,1}^{\max}$ a minimal perturbation is sufficient to make $\varphi_{1,1}$ move either to the right or to the left minimum

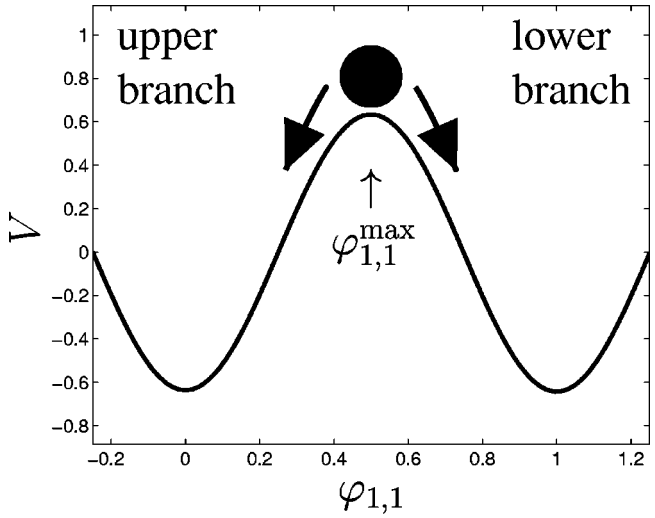

FIG. 6. The potential V from (18) governs the dynamics of the normalized cyclic phase difference $\varphi_{1,1}$ according to (17) and (19). Starting at the potential's maximum, a slight perturbation may drive $\varphi_{1,1}$ down to either the right or to two left minimum, which corresponds to running through the lower or upper branch shown in Fig. 2(f). The maximum of V is located in $\varphi_{1,1}^{\max}$. [Because of the graphics program used, in Fig. 2(f) the y-axis runs downwards, so that values of $\varphi_{1,1}$ in the upper branch are smaller than those in the lower branch.]

of V. Depending on whether $\varphi_{1,1}$ is greater or less than $\varphi_{1,1}^{\max}$, the particle relaxes into the right or left minimum, respectively. Hence, by placing $\varphi_{1,1}$ to the right or to the left of $\varphi_{1,1}^{\max}$, the stimulus completely determines whether $\varphi_{1,1}$ moves to the right or to the left minimum.

The situation is qualitatively different when noise is added, i.e., for $D>0$. Instead of predicting the trajectory of the particle, the dynamics can now only be described in a probabilistic sense. For instance, by means of a Fokker–Planck equation we can determine the time course of the probability density $p(\varphi_{1,1},t)$, where $p(\varphi_{1,1},t)\mathrm{d}\varphi_{1,1}$ gives us the probability of finding $\varphi_{1,1}$ in the interval $[\varphi_{1,1},\varphi_{1,1}+\mathrm{d}\varphi_{1,1}]$ (see Ref. 1 and Chap. 9 in Ref. 22). Noise influences the dynamics both during and after stimulation.

The impact of noise during stimulation: In the absence of noise, the same stimulus applied to the oscillators in the same dynamical state always moves the particle to the same place in the potential V. In contrast, in the presence of noise the motion of the particle is perturbed by random forces, so that the outcome of the stimulus can no longer be predicted precisely, but only in terms of a probability. In other words, applying the same stimulus to the same dynamical state several times, leads to a noise-induced scattering of the position of the particle at the end of the stimulation.

The impact of noise after stimulation: The overdampled motion of the particle is perturbed by random forces and behaves in a way which has been studied in detail in the context of diffusion in a double-well potential (see Chap. 9 in Ref. 22). The dynamics for $t\to\infty$ is no longer totally determined by the initial state, which means that the division into three different scenarios (i.e., staying at the unstable maximum or moving into the right or left minimum) is no longer valid. For sufficiently large noise amplitude the particle may end up in the right well although it started left from $\varphi_{1,1}^{\max}$ and vice versa.

B. Detection of symmetric cross-trial antiphase response clustering

In Sec. IV we have seen, that the poststimulus cross-trial branching of the phase difference $\varphi_{1,1}$ is tightly related to a cross-trial antiphase clustering of the phase ϕ_j of each oscillator. The poststimulus cross-trial clustering of ϕ_j shown in Figs. 2 and 3 is symmetrical, which means that the number of responses in both clusters are approximately the same. Accordingly, $\overline{x_j^a}$ and $\overline{x_j^b}$, i.e., the averaged responses belonging to each of the two clusters, have approx. the same amplitude, so that $\overline{x_j}=(\overline{x_j^a}+\overline{x_j^b})/2$ vanishes as soon as the antiphase relationship between $\overline{x_j^a}$ and $\overline{x_j^b}$ is established [see Figs. 3(h), 3(j)].

To study the impact of noise on the averaged reponses $\overline{x_1}$ and $\overline{x_2}$, it is necessary to investigate under which conditions a symmetric antiphase poststimulus response clustering occurs. With this aim in view we introduce the time-dependent *antiphase clustering index* of the jth oscillator by setting

$$\alpha_j(t)=\lambda_j^{(2)}(t)-\lambda_j^{(1)}(t). \tag{20}$$

$-1\leqslant\alpha_j(t)\leqslant 1$ is fulfilled for all times t. $\alpha_j(t)$ specifically detects symmetric cross-trial antiphase response clustering which is stimulus locked in time. To illustrate this, let us define the *time-dependent configuration of a cross-trial 2-cluster state*. We assume that an ensemble of l responses of the jth oscillator at time t relative to the stimulus onset splits into two groups, which consist of $l_1(t)$ and $l_2(t)$ responses, respectively. Within each group the phase difference between the different repsonses at time t is small, whereas the mean phase difference between the two groups at time t is large, e.g., close to π. The configuration of the cross-trial 2-cluster state at time t will be denoted by $[l_1(t),l_2(t)]$. The definition of the configuration of a cross-trial 2-cluster state corresponds to the definition of the configuration of a 2-cluster state in a population of coupled oscillators.[23]

To illustrate the configuration of a cross-trial 2-cluster state let us consider an ensemble of simple synthetic responses of the jth oscillator defined by

$$\phi_j(t+\tau_k)=[t+\varepsilon\xi_k] \mod 1 \quad (k=1,\ldots,l_1), \tag{21}$$

$$\phi_j(t+\tau_k)=[t+0.5+\varepsilon\xi_k] \mod 1 \quad (k=l_1+1,\ldots,l), \tag{22}$$

where $\{\xi_k\}_{k=1}^{l}$ is constant in time and normally distributed with unit variance. The variance of the distribution of the responses is modified by varying ε. For vanishing ε the responses belonging to each cluster are identical, respectively, and the only difference between the two clusters is their antiphase relationship. In the simple example given by Eqs. (21) and (22) the configuration $[l_1(t),l_2(t)]$ is not time-dependent. Note, the responses given by Eqs. (21) and (22) are not obtained by integrating model equation (1) numerically. Rather, for the sake of illustration these responses are simply defined by Eqs. (21) and (22) and, of course, they are artificial, but they serve their purpose.

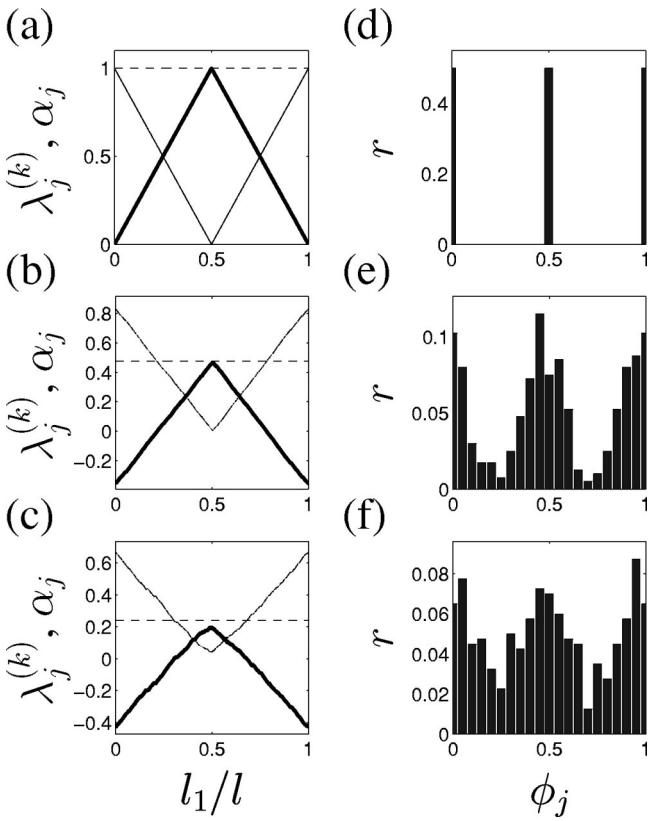

FIG. 7. Antiphase cross-trial 2-cluster states are formed by the synthetic responses of the jth oscillator as defined by Eqs. (21) and (22): The l_1 responses of the first cluster read $\phi_j(t+\tau_k)=[t+\varepsilon\xi_k] \bmod 1$ for $k=1,\ldots,l_1$, whereas the l_2 responses of the second cluster read $\phi_j(t+\tau_k)=[t+0.5+\varepsilon\xi_k] \bmod 1$ for $k=l_1+1,\ldots,l$, where $l_1+l_2=l=400$. We analyze 2-cluster states for $t=1$. In (a)–(c) the extent of asymmetry of the antiphase cross-trial 2-cluster is varied by varying l_1/l, i.e., the ratio of the number of responses of the first cluster l_1 to the total number of responses l. $\{\xi_k\}_{k=1}^{l}$ is constant in time and normally distributed with unit variance for all values of l_1/l. The variance of the responses is modified by varying ε: $\varepsilon=0$ in (a), $\varepsilon=\sqrt{0.01}$ in (b), and $\varepsilon=\sqrt{0.02}$ in (c). Put otherwise, the overall variance of $\varepsilon\{\xi_k\}_{k=1}^{l}$ in (a), (b), and (c) is 0, 0.01, and 0.02. Cross-trial antiphase response clustering is detected by means of $\alpha_j=\lambda_j^{(2)}-\lambda_j^{(1)}$, the antiphase clustering index of the jth oscillator defined by (20). α_j (bold line), $\lambda_j^{(1)}$ from (8) (thin line), and $\lambda_j^{(2)}$ from (9) (dashed line) are displayed in (a)–(c). In (d)–(f) the corresponding distributions of the phases ϕ_j are plotted for the symmetric configuration, i.e., for $l_1=l_2$, where (d) belongs to (a), (e) to (b), and (f) to (c). The number of bins N_{bin} is determined according to the formula $N_{\text{bin}}=\exp[0.626+0.4\log(l-1)]$ (Ref. 24) and, hence, equals 21. The relative frequency r, which is the ratio of the number of responses ϕ_j within a particular bin to the total number of reponses l is displayed in (d)–(f). For the responses $\phi_j(t+\tau_k)$ under consideration the indices α_j, $\lambda_j^{(1)}$, and $\lambda_j^{(2)}$ shown in (a)–(c) are time-independent, whereas increasing t causes a linear shift mod 1 of the distributions displayed in (d)–(f).

Figure 7 shows α_j from (20), $\lambda_j^{(1)}$ from (8), and $\lambda_j^{(2)}$ from (9) for different values of ε, where the ratio l_1/l of the number of responses of the first cluster l_1 to the total number of responses l is varied between 0 and 1. Varying l_1/l means modifying the extent of asymmetry of the antiphase cross-trial 2-cluster state. A perfectly symmetric antiphase cross-trial 2-cluster state consists of two clusters which are the same size and, thus, fulfill $l_1=l_2$ and $l_1/l=0.5$. Figure 7 visualizes the two main factors that determine the value of the antiphase clustering index: $\alpha_j(t)$ is the larger (i) the more symmetrical the cross-trial 2-cluster state and (ii) the smaller the variance within the two clusters. In other words, $\alpha_j(t)$ specifically detects distinct symmetric cross-trial 2-cluster states of the responses of a single oscillator at time t relative to stimulus onset.

C. Stimulus-locked dynamics with no noise

Figures 8 and 9 show the dynamics caused by the same stimuli $S_1(\psi_1)=I\cos\psi_1$ and $S_2(\psi_2)=I\cos(\psi_2+\pi)$ as in Fig. 2, which are applied to the two oscillators modeled by Eq. (1), where the noise amplitude D now vanishes. We consider the noise-free case with and without frequency detuning μ, where the eigenfrequencies are given by $\omega_{1,2}=\omega\pm\mu/2$. $D=\mu=0$ in Fig. 8, whereas $D=0$ and $\mu=0.5$ in Fig. 9.

Let us first dwell on the *noise-free case without frequency detuning* ($D=\mu=0$, Fig. 8): Without stimulation the two oscillators are strongly synchronized in-phase [Figs. 8(j), 8(k)]. An antiphase reset is rapidly achieved by means of the two strong stimuli: After the stimulation ϕ_1 is close to $\phi_1^{\text{stat}}\approx 0.36$ [Fig. 8(a)], whereas ϕ_2 is close to $\phi_2^{\text{stat}}=\phi_1^{\text{stat}}+0.5\approx 0.86$ [Fig. 8(f)]. The antiphase reset is a consequence of the phase shift of π in the argument of S_2 (see also Fig. 2). Since there is no noise, $\varphi_{1,1}$ relaxes from the maximum of the potential V to a minimum of V only slowly (Fig. 6, see Sec. 9.1.5 in Ref. 22). Accordingly, the transition from antiphase synchronization to in-phase synchronization takes much longer in the noise-free case [Fig. 8(j), cf. Fig. 2(f)].

For vanishing detuning the potential V from (18) is symmetrical about the line $\varphi_{1,1}=0.5$ [Fig. 10(a)]. The antiphase reset places $\varphi_{1,1}$ on top of the potential's maximum or very close to it. Let us denote the time at the end of the stimulation by t_{off}. The stimulus is not infinitely long, so that the antiphase reset is not perfect. This is why at the end of the stimulation the cross-trial distribution of $\varphi_{1,1}(t_{\text{off}})$ splits into two peaks which are located to the right and to the left of $\varphi_{1,1}^{\max}$, respectively [Fig. 10(b)]. For higher stimulation duration, e.g., for twice the duration, the two peaks melt and form one peak with a maximum at $\varphi_{1,1}^{\max}$ (not shown for space constraints). As explained in Sec. VIII A, after the stimulation $\varphi_{1,1}$ moves to the left well of the potential V if $\varphi_{1,1}(t_{\text{off}})<\varphi_{1,1}^{\max}$ [Fig. 11(a)], whereas $\varphi_{1,1}$ moves to the right well if $\varphi_{1,1}(t_{\text{off}})>\varphi_{1,1}^{\max}$ [Fig. 11(b)]. The cross-trial branching of $\varphi_{1,1}$ is connected with a cross-trial antiphase clustering of ϕ_j which is connected with a relaxation of $\lambda_j^{(1)}$ [Fig. 8(b)] and a reincrease of $\lambda_j^{(2)}$ [Figs. 8(c), 8(g)]. The symmetric antiphase cross-trial response clustering leads to a relaxation of the cross-trial averaged signal $\overline{x_j}$ from (11) [Figs. 8(e), 8(i)] and is detected with the antiphase clustering index α_j defined by Eq. (20) [Figs. 8(d), 8(h)].

Next, we consider the *noise-free case with frequency detuning* ($D=0$, $\mu=0.5$, Fig. 9): Without stimulation the two oscillators are strongly synchronized in-phase [Figs. 9(j), 9(k)]. The stimuli S_1 and S_2 perform a rapid antiphase reset. Due to the frequency detuning the potential V is no longer symmetrical about the line $\varphi_{1,1}=0.5$: The right well is deeper than the left well, and the maximum of the potential V is now located in $\varphi_{1,1}^{\max}=0.499\,75$ [Fig. 10(a)]. Consequently, in only a few of the trials $\varphi_{1,1}(t_{\text{off}})$ is located to the

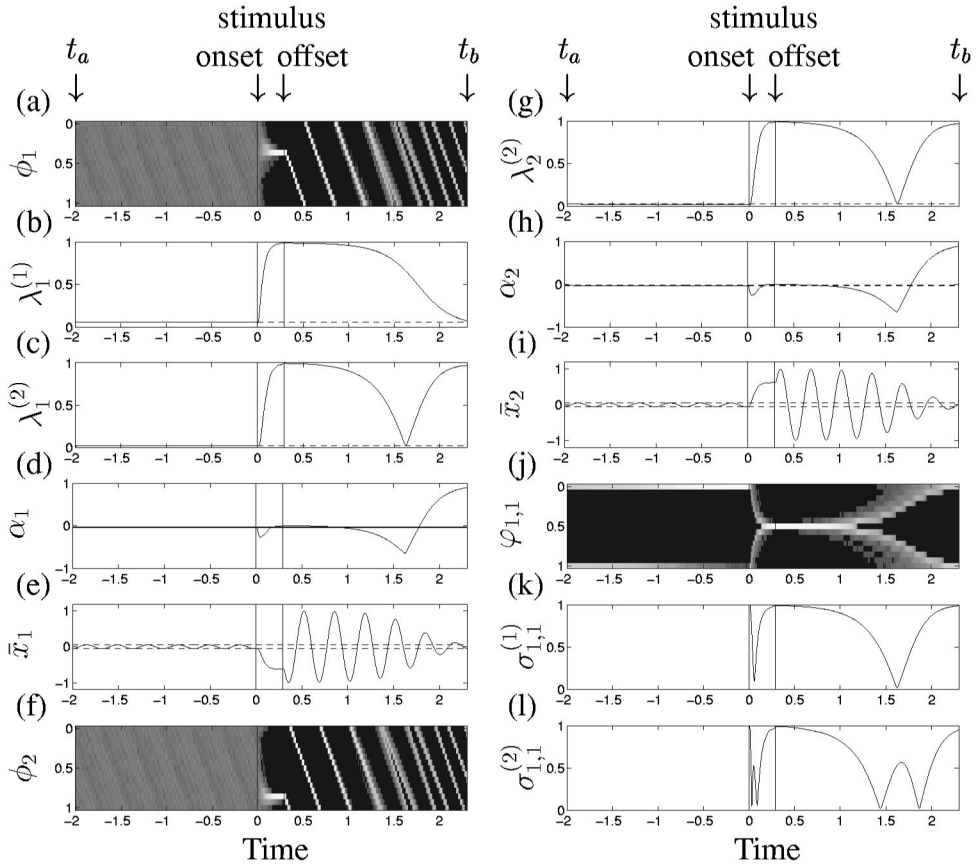

FIG. 8. The same stimuli $S_1(\psi_1) = I\cos\psi_1$ and $S_2(\psi_2) = I\cos(\psi_2+\pi)$ as in Fig. 2 are applied to the two oscillators given by Eq. (1). In contrast to Fig. 2, in this simulation there is no noise ($D=0$) and no frequency detuning ($\mu=0$), so that the eigenfrequencies of both oscillators coincide ($\omega_1=\omega_2$). CT distributions $\{\phi_1(t+\tau_k)\}_{k=1,\ldots,I}$, $\{\phi_2(t+\tau_k)\}_{k=1,\ldots,I}$, and $\{\varphi_{1,1}(t+\tau_k)\}_{k=1,\ldots,I}$ are shown in in (a), (f), and (j), respectively. Locking indices from Eqs. (8) and (9): $\lambda_1^{(1)}$ in (b), $\lambda_1^{(2)}$ in (c), and $\lambda_2^{(2)}$ in (g). $\lambda_2^{(1)}$ and $\lambda_1^{(1)}$ nearly coincide. $\sigma_{1,1}^{(1)}$ and $\sigma_{1,1}^{(2)}$ are displayed in (k) and (l). Cross-trial averaged signals $\overline{x_1}$ in (e) and $\overline{x_2}$ in (i) are calculated according to Eq. (11), with the 99th and first percentile of $\{\overline{x_j}(t)\}_{t\in[-2,0[}$ indicated by upper and lower dashed lines. 99th and first percentile practically lie on top of each other. Same format as in Fig. 2. Parameters of Eq. (1) as in Fig. 2, except for the noise amplitude $D=0$ and the frequency detuning $\mu=0$.

left of $\varphi_{1,1}^{\max}$ [Fig. 10(c)]. Therefore, in the majority of trials $\varphi_{1,1}$ decays to the right well of the potential V [Fig. 9(j)]. Since there is practically no cross-trial branching of $\varphi_{1,1}$, there is also no relevant cross-trial response clustering [Figs. 9(a), 9(f)]: Hence, $\lambda_j^{(1)}$ does not relax [Fig. 9(b)], and α_j does not increase [Figs. 9(d), 9(h)]. Correspondingly, also the cross-trial averaged signal $\overline{x_j}$ does not relax [Figs. 9(e), 9(i)].

D. Stimulus-locked dynamics with noise

We run a simulation with the detuned oscillators from Fig. 9, but now we introduce noise ($D=0.5$). As discussed in Sec. VIII A this causes two effects:

(1) *Effect of noise during stimulation:* While in the noise-free case in the ensemble of responses $\varphi_{1,1}(t_{\text{off}})$ is mainly located to the right of $\varphi_{1,1}^{\max}$ [Fig. 10(c)], noise broadens the cross-trial distribution of $\varphi_{1,1}(t_{\text{off}})$, so that in approx. half of the trials $\varphi_{1,1}<\varphi_{1,1}^{\max}$ and vice versa [Fig. 10(d)].

(2) *Effect of noise after stimulation:* In the noise-free case $\varphi_{1,1}$ moves to the left potential well if $\varphi_{1,1}(t_{\text{off}})<\varphi_{1,1}^{\max}$ [Fig. 11(a)], whereas $\varphi_{1,1}$ moves to the right well if $\varphi_{1,1}(t_{\text{off}})>\varphi_{1,1}^{\max}$ [Fig. 11(b)]. In contrast, in the presence of noise $\varphi_{1,1}$ may either move to the right or to the left well, regardless of whether $\varphi_{1,1}(t_{\text{off}})<\varphi_{1,1}^{\max}$ [Fig. 11(c)] or $\varphi_{1,1}(t_{\text{off}})>\varphi_{1,1}^{\max}$ [Fig. 11(d)].

These two effects guarantee that—different from the noise-free case—we now observe a cross-trial response clustering of ϕ_j for both $\varphi_{1,1}(t_{\text{off}})<\varphi_{1,1}^{\max}$ [Fig. 11(e)] and $\varphi_{1,1}(t_{\text{off}})>\varphi_{1,1}^{\max}$ [Fig. 11(f)].

E. Stochastic resonance of transient response clustering

In Secs. VIII C and VIII D we have seen that in identical oscillators symmetric cross-trial antiphase response clustering occurs already for vanishing noise amplitude D, whereas sufficiently detuned oscillators need a certain amount of noise in order to exhibit this dynamical phenomenon.

To study the relationship between noise amplitude and the extent of symmetric antiphase response clustering in detuned oscillators we introduce two quantities: We obtain the *mean poststimulus antiphase clustering index* of the jth oscillator by averaging $\alpha_j(t)$ from Eq. (20) over the poststimulus interval $[t_{\text{off}},t_b]$ according to

$$\overline{\alpha_j}=\frac{1}{t_b-t_{\text{off}}}\int_{t_{\text{off}}}^{t_b}\alpha_j(\xi)\,\mathrm{d}\xi. \tag{23}$$

Analogously the *maximal post-stimulus anti-phase clustering index* of the jth oscillator reads

$$\alpha_j^{\max}=\max\{\alpha_j(t);t\in[t_{\text{off}},t_b]\}. \tag{24}$$

Again we turn to the oscillators with detuning $\mu=0.5$, which were shown in the simulation from Fig. 9. Model equation (1) is now integrated numerically with noise amplitude D varying between 0 and 1.5 (Fig. 12). For $D=0$ the cross-trial

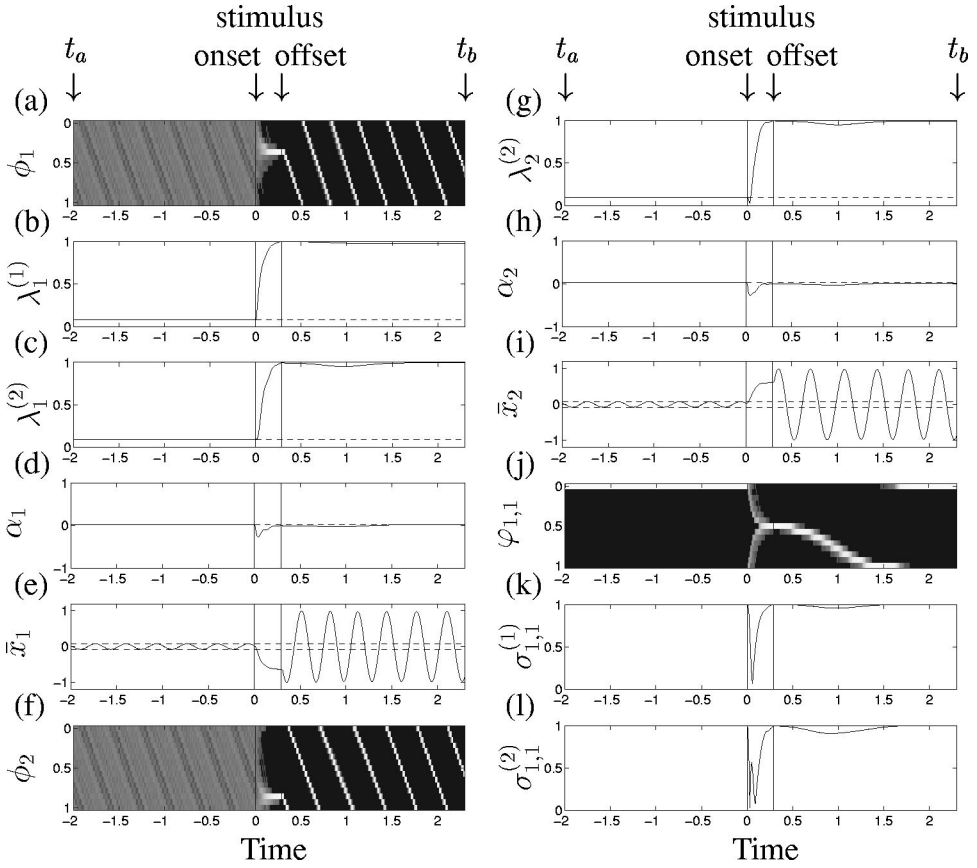

FIG. 9. The same stimuli $S_1(\psi_1)=I\cos\psi_1$ and $S_2(\psi_2)=I\cos(\psi_2+\pi)$ as in Figs. 2 and 8 are administered to the two oscillators given by Eq. (1). The simulation shown in Fig. 8 was performed for vanishing noise amplitude ($D=0$) and vanishing detuning ($\mu=0$). In contrast, in this simulation the eigenfrequencies of the two oscillators are detuned with $\mu=0.5$. CT distributions $\{\phi_1(t+\tau_k)\}_{k=1,\ldots,l}$, $\{\phi_2(t+\tau_k)\}_{k=1,\ldots,l}$, and $\{\varphi_{1,1}(t+\tau_k)\}_{k=1,\ldots,l}$ are shown in in (a), (f), and (j), respectively. Locking indices from Eqs. (8) and (9): $\lambda_1^{(1)}$ in (b), $\lambda_1^{(2)}$ in (c), and $\lambda_2^{(2)}$ in (g). $\lambda_2^{(1)}$ and $\lambda_1^{(1)}$ nearly coincide. $\sigma_{1,1}^{(1)}$ and $\sigma_{1,1}^{(2)}$ are displayed in (k) and (l). Cross-trial averaged signals $\overline{x_1}$ and $\overline{x_2}$ are shown in (e) and (i). Same format as in Fig. 8. Parameters of Eq. (1) as in Fig. 8, except for the detuning $\mu=0.5$.

averaged response $\overline{x_j}$ and the corresponding index $\lambda_j^{(1)}$ relax only very slowly [Figs. 12(a), 12(b)]. With increasing D we observe a much quicker relaxation of both $\overline{x_j}$ and $\lambda_j^{(1)}$ [Figs. 12(a), 12(b)]. The antiphase response clustering is reflected by a reincrease of $\lambda_j^{(2)}$ [Fig. 12(c)] and—more specifically—by an epoch with positive antiphase clustering index α_j, which indicates a pronounced symmetric antiphase response clustering [Fig. 12(d)]. This clustering is particularly strong for values of D approximately between 0.2 and 0.7.

Stochastic resonance of symmetric cross-trial antiphase response clustering is demonstrated by plotting $\overline{\alpha_j}$ over the noise amplitude D [Fig. 12(e)] and, in particular, by plotting $\alpha_j^{\max}$ over D [Fig. 12(e)]. Without noise there is no response clustering. For intermediate values of the noise amplitude (i.e., D around 0.25) the response clustering is strongest, whereas with further increasing D the extent of reponse clustering decreases again. A noise-dependence of this kind is a feature which is typical for stochastic resonance.[25] The stochastic resonance effect is more distinct for $\alpha_j^{\max}$ than for $\overline{\alpha_j}$ [Figs. 12(e), 12(f)], because the period, during which the pronounced symmetric response clustering occurs, is clearly smaller than the duration of the poststimulus interval $[t_{\text{off}},t_b]$ chosen in Fig. 12(d).

IX. DISCUSSION

In this work, I have introduced a model which allows to study transient phase dynamics, synchronization, and desynchronization of two coupled phase oscillators. Furthermore, appropriate data analysis tools have been presented which make it possible to detect these transient dynamical processes both in simulated and experimental data. These novel data analysis tools have been compared to standard data analysis techniques, applied in a cross-trial manner. Cross-trial cross-correlation inevitably causes massive artifacts in terms of artificial oscillations that are not related to synchronization or desynchronization processes [Figs. 3(l)–3(n)]. Cross-trial averaging as used in evoked response studies[6,13,14] may lead to severe misinterpretations since it cannot distinguish between transient response clustering and an overall decrease of the amplitude of the single responses (Figs. 3–5).

Response decorrelation due to transient antiphase clustering is robust with respect to variations of the model parameters: It is neither restricted to symmetric stimulation intensities and couplings nor to in-phase coupling (as can be seen with the transformation $\psi_j\to\psi_j+c_j$ with constant c_j). Effects of asymmetries of coupling and stimulation, higher

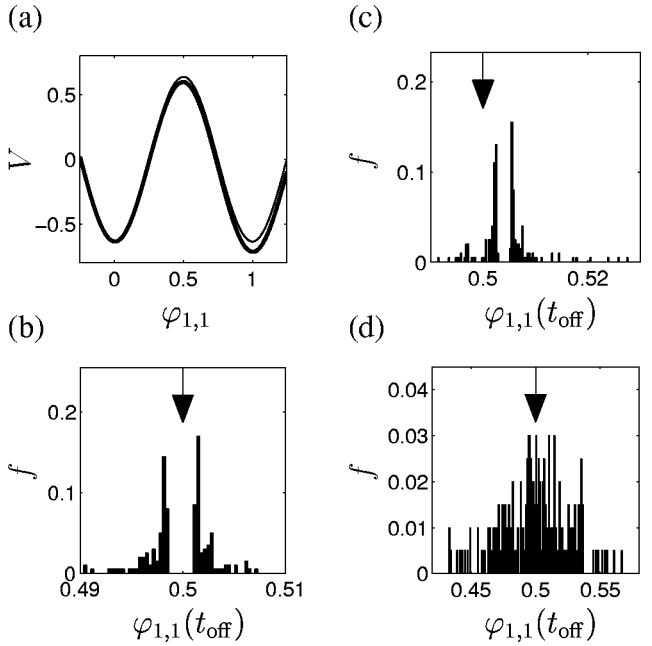

FIG. 10. The potential V from Eq. (18) is plotted in (a) for the detuned oscillators ($\mu=0.5$, bold line) and for identical oscillators ($\mu=0$, thin line), where in both cases $K=2$. The distribution of $\varphi_{1,1}(t_{\mathrm{off}})$, i.e., the distribution of $\varphi_{1,1}$ at the end of the stimulation t_{off}, is shown for three different cases: no noise and no detuning ($D=0$, $\mu=0$) in (b), no noise and detuning ($D=0$, $\mu=0.5$) in (c), noise and detuning ($D=0.5$, $\mu=0.5$) in (d). In (b)–(d) the vertical arrow indicates $\varphi_{1,1}^{\max}$, the location of the maximum of the potential V. (b), (c), and (d) belong to the simulations displayed in Figs. 8, 9, and 11(c)–11(f), respectively.

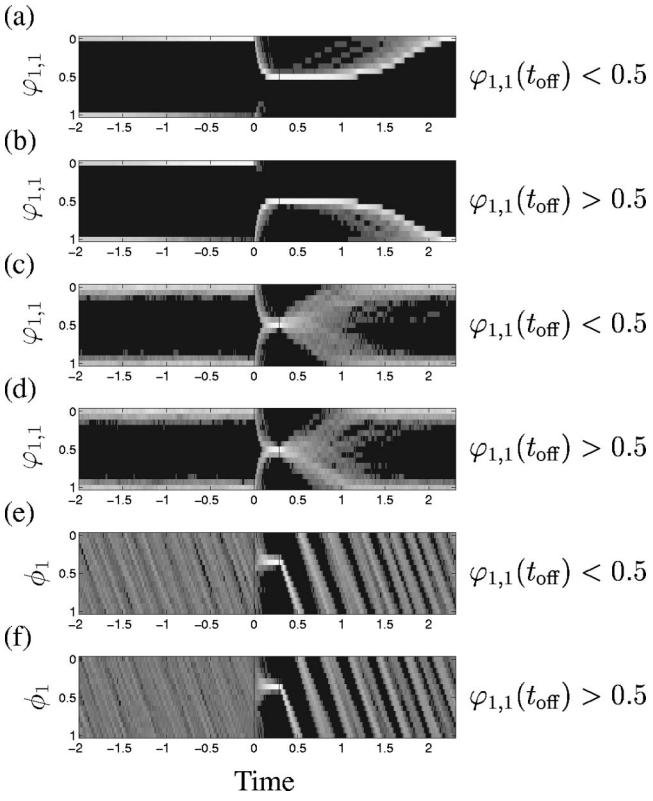

FIG. 11. The CT distribution $\{\varphi_{1,1}(t+\tau_k)\}_{k=1,\ldots,I}$ from Fig. 8(j) is divided into the CT distribution $\{\varphi_{1,1}(t+\tau_k)\}$ of the trials fulfilling $\varphi_{1,1}(t_{\mathrm{off}})<0.5$ (a) and the CT distribution $\{\varphi_{1,1}(t+\tau_k)\}$ of the trials with $\varphi_{1,1}(t_{\mathrm{off}})>0.5$ (b). The simulation shown in Fig. 9 was additionally performed with nonvanishing noise amplitude $D=0.5$. The CT distribution $\{\varphi_{1,1}(t+\tau_k)\}$ of the trials fulfilling $\varphi_{1,1}(t_{\mathrm{off}})<0.5$ is shown in (c) and the CT distribution $\{\varphi_{1,1}(t+\tau_k)\}$ of the trials with $\varphi_{1,1}(t_{\mathrm{off}})>0.5$ in (d). Furthermore, for this noisy simulation the CT distributions $\{\phi_1(t+\tau_k)\}$ of the trials with $\varphi_{1,1}(t_{\mathrm{off}})<0.5$ is displayed in (e) and the CT distribution $\{\phi_1(t+\tau_k)\}$ of the trials with $\varphi_{1,1}(t_{\mathrm{off}})>0.5$ is shown in (f). In (a)–(f) black corresponds to minimal values, whereas white corresponds to maximal values.

order coupling and stimulation terms, delays and stimuli applied at different times will be presented soon.

If the stimuli S_j are not strong enough, i.e., if intensity I and/or stimulation duration are not large enough, the analysis has to be performed for different values of the initial phases $\phi_j(0)$ separately with a suitable binning of $\phi_j(0)$ to determine the impact of the initial conditions. In this way the impact of the initial phase at the beginning of the stimulation on the outcome of the stimulation can be revealed (cf. Ref. 5).

Noise plays a crucial role in the emergence of stimulus-locked symmetric antiphase response clustering. In identical oscillators (i.e., with vanishing detuning μ) the response clustering occurs also in the absence of noise (Fig. 8). Without noise and with small detuning the clustering of ϕ_j is strongly asymmetrical, so that $\overline{x_j}$ vanishes slowly in time. Without noise and with sufficiently large detuning there is no response clustering any more (Fig. 9). However, sufficiently strong noise causes a symmetric response clustering also in detuned oscillators (Fig. 11). In fact, the mechanism by which noise induces symmetric antiphase cross-trial response clustering in detuned oscillators is a stochastic resonance (Fig. 12). Since in many applications, e.g., in biology, one typically encounters detuned oscillators, the inherent noise modeled by the random forces $F_j(t)$ in Eq. (1) has to be considered essential for the generation of transient stimulus-locked dynamical processes like transient symmetric antiphase response clustering. Inherent noise generates transient dynamical order, and as a consequence of the attempt to average out this type of noise, e.g., with cross-trial averaging as defined by Eq. (11), one will inevitably miss important transient processes.

Transient antiphase clustering may, e.g., enable the nervous system to switch between different coordinated reactions to the same stimulus. This may be an essential mechanism necessary for short-term adaptation in sensory information processing. The data analysis approach presented in Sec. III provides a key for the study of the interactions of oscillators during stimulus-locked transient short-term dynamics with a superb time resolution. It prevents from misinterpretations originating from the standard cross-trial averaging as well as the cross-trial cross-correlation analysis and is already being applied to EEG/MEG signals and to the cerebral current source density.

In an application to experimental data also the oscillators' amplitudes have to be registered. To investigate the stimulus-locked dynamics one can either average them across trials as done in Eq. (11) with the signals or one can evaluate the cross-trial distribution of the amplitudes in a similar way as defined by Eqs. (8) and (9) for the phases. This was not necessary here, since the amplitude of the phase oscillators is constant. In experimental data a relevant oscil-

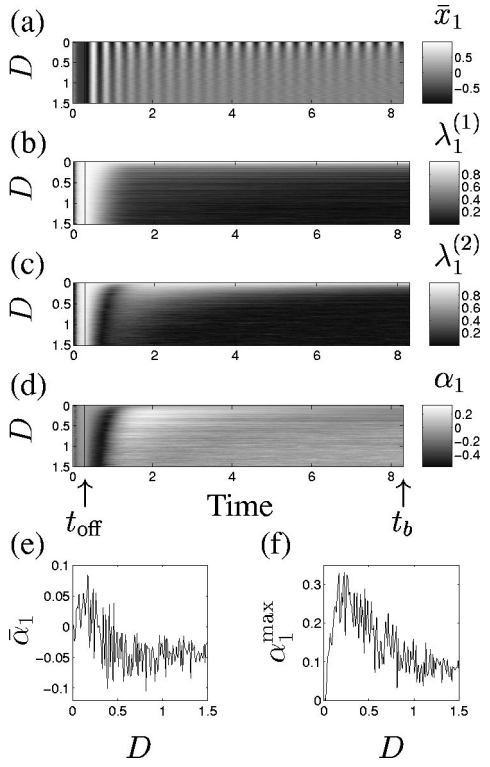

FIG. 12. The simulation from Figs. 11(c)–11(f) was performed for different values of the noise amplitude D, while all other model parameters remained unchanged. The cross-trial averaged signal $\overline{x_1}$ is shown in (a), $\lambda_1^{(1)}$ in (b), $\lambda_1^{(2)}$ in (c), and the antiphase clustering index of the first oscillator $\alpha_1 = \lambda_1^{(2)} - \lambda_1^{(1)}$ from Eq. (20) in (d). $\lambda_2^{(1)}$, $\lambda_2^{(2)}$, and α_2 nearly coincide with $\lambda_1^{(1)}$, $\lambda_1^{(2)}$, and α_1, respectively. Stochastic resonance of the transient symmetric poststimulus antiphase response clustering is illustrated by plotting $\overline{\alpha_1}$, the mean poststimulus antiphase clustering index of the first oscillator, in (e) and $\alpha_1^{\max}$, the maximal poststimulus antiphase clustering index, in (f). $\overline{\alpha_1}$ and $\alpha_1^{\max}$ are evaluated in the poststimulus interval $[t_{off}, t_b]$ according to Eqs. (23) and (24), respectively. Number of stimuli $l = 400$.

latory signal $s(t)$ such as a particular brain rhythm is extracted out of a complex Fourier spectrum with bandpass filtering. A filter causing a phase shift of $\pi/2$ for all frequencies yields the Hilbert transform $s_H(t)$ of $s(t)$ and instantaneous phase $\psi(t)$ and amplitude $A(t)$ of $s(t)$ according to $s(t) + s_H(t) = A(t)\exp[i\psi(t)]$.[26] For discrete signals like timing sequences of spiking neurons the phase can be estimated with linear interpolation.

From the physiological standpoint it should be mentioned that the shape of stimulus locked oscillatory responses, the so-called waveform of the response, crucially depends on the interactions between different oscillators (Fig. 4). As a consequence of the oscillators' interactions, equating the amplitude of the stimulus-locked cross-trial averaged response $\overline{x_j}$ with a stimulus-locked "activity" of the jth oscillator causes massive misinterpretations. It is, thus, indispensable to study transient stimulus-locked coordinated dynamics appropriately in order to reveal transient dynamical processes and their potential meaning, e.g., in terms of mechanisms of short-term adaptation in sensory processing.

[1] H. Haken, *Advanced Synergetics* (Springer, Berlin, 1983).
[2] Y. Kuramoto, *Chemical Oscillations, Waves, and Turbulence* (Springer, Berlin, 1984).
[3] A. T. Winfree, *The Geometry of Biological Time* (Springer, Berlin, 1980).
[4] H. Steriade, E. G. Jones, and R. Llinás, *Thalamic Oscillations and Signaling* (Wiley, New York, 1990).
[5] P. A. Tass, *Phase Resetting in Medicine and Biology: Stochastic Modeling and Data Analysis* (Springer, Berlin, 1999).
[6] K. H. Chiappa, *Evoked Potentials in Clinical Medicine* (Raven, New York, 1983).
[7] A. S. Pikovsky, M. G. Rosenblum, and J. Kurths, "Phase synchronization in a population of globally coupled chaotic oscillators," Europhys. Lett. **34**, 165–170 (1996).
[8] M. G. Rosenblum, A. S. Pikovsky, and J. Kurths, "Phase synchronization of chaotic oscillators," Phys. Rev. Lett. **76**, 1804–1807 (1996).
[9] A. S. Pikovsky, M. G. Rosenblum, and J. Kurths, *Synchronization: A Universal Concept in Nonlinear Sciences* (Cambridge University Press, Cambridge, 2001).
[10] P. Tass, M. G. Rosenblum, J. Weule, J. Kurths, A. Pikovsky, J. Volkmann, A. Schnitzler, and H.-J. Freund, "Detection of $n:m$ phase locking from noisy data: Application to magnetoencephalogray," Phys. Rev. Lett. **81**, 3291–3294 (1998).
[11] A. Neiman, L. Schimansky-Geier, A. Cornell-Bell, and F. Moss, "Noise-enhanced phase synchronization in excitable media," Phys. Rev. Lett. **83**, 4896–4899 (1999).
[12] R. L. Stratonovich, *Topics in the Theory of Random Noise* (Gordon and Breach, New York, 1963).
[13] G. D. Dawson, "A summation technique for the detection of small evoked potentials," Electroencephalogr. Clin. Neurophysiol. **44**, 153–154 (1954).
[14] M. Hämäläinen, R. Hari, R. J. Ilmoniemi, J. Knuutila, and O. V. Lounasmaa, "Magnetoencephalography: Theory, instrumentation, and applications to noninvasive studies of the working human brain," Rev. Mod. Phys. **65**, 413–497 (1993).
[15] P. A. Tass, "Stimulus-locked transient phase dynamics, synchronization and desynchronization of two oscillators," Europhys. Lett. **59**, 199–205 (2002).
[16] H. Daido, "Order function and macroscopic mutual entrainment in uniformly coupled limit-cycle oscillators," Prog. Theor. Phys. **88**, 1213–1218 (1992).
[17] R. Hari and R. Salmelin, "Human cortical oscillations: a neuromagnetic view through the skull," Trends Neurosci. **20**, 44–49 (1997).
[18] B. Sayers, H. A. Beagley, and W. R. Hanshall, "The mechanisms of auditory evoked EEG responses," Nature (London) **247**, 481–483 (1974).
[19] S. Makeig, M. Westerfield, T.-P. Jung, S. Enghoff, J. Townsend, E. Courchesne, and T. J. Sejnnowski, "Dynamic brain sources of visual evoked responses," Science **295**, 690–694 (2002).
[20] *Handbook of Biological Physics Vol. IV*, edited by C. Gielen and F. Moss (Elsevier, Amsterdam, 2001).
[21] J. Bendat and A. Piersol, *Random Data: Analysis and Measurement Procedures*, 3rd ed. (Wiley, New York, 2000).
[22] C. W. Gardiner, *Handbook for Stochastic Methods for Physics, Chemistry, and the Natural Sciences*, 2nd ed. (Springer, Berlin, 1985).
[23] P. Tass, "Phase and frequency shifts in a population of phase oscillators," Phys. Rev. E **56**, 2043–2060 (1997).
[24] R. K. Otnes and L. Enochson, *Digital Time Series Analysis* (Wiley, New York, 1972).
[25] L. Gammaitoni, P. Hänggi, P. Jung, and F. Marchesoni, "Stochastic resonance," Rev. Mod. Phys. **70**, 223–287 (1998).
[26] P. Panter, *Modulation, Noise, and Spectral Analysis* (McGraw–Hill, New York, 1965).